RIVER RESEARCH AND APPLICATIONS

River. Res. Applic. **24**: 1160–1174 (2008)

Published online 22 April 2008 in Wiley InterScience
(www.interscience.wiley.com) DOI: 10.1002/rra.1122

EROSION PROPERTIES OF COHESIVE SEDIMENTS IN THE COLORADO RIVER IN GRAND CANYON

RYOSUKE AKAHORI,[a] MARK W. SCHMEECKLE,[a]* DAVID J. TOPPING[b] and THEODORE S. MELIS[b]

[a] *School of Geographical Sciences, Arizona State University, AZ, USA*
[b] *U.S. Geological Survey, Grand Canyon Monitoring and Research Center, AZ, USA*

ABSTRACT

Cohesive sediment deposits characterized by a high fraction of mud (silt plus clay) significantly affect the morphology and ecosystem of rivers. Potentially cohesive sediment samples were collected from deposits in the Colorado River in Marble and Grand Canyons. The erosion velocities of these samples were measured in a laboratory flume under varying boundary shear stresses. The non-dimensional boundary shear stress at which erosion commenced showed a systematic deviation from that of non-cohesive sediments at mud fractions greater than 0.2. An empirical relation for the boundary shear stress threshold of erosion as a function of mud fraction was proposed. The mass erosion rate was modelled using the Ariathurai–Partheniades equation. The erosion rate parameter of this equation was found to be a strong function of mud fraction. Under similar boundary shear stress and sediment supply conditions in the Colorado River, cohesive lateral eddy deposits formed of mud fractions in excess of 0.2 will erode less rapidly than non-cohesive deposits. Copyright © 2008 John Wiley & Sons, Ltd.

KEY WORDS: cohesive sediment; flume experiments; Grand Canyon; sediment transport; mud; erosion

Received 27 September 2007; Revised 16 January 2008; Accepted 1 February 2008

INTRODUCTION

Cohesive sediments have profound effects on the morphology of rivers and on riparian ecosystem function. Empirically it has been shown that streams having banks with high silt–clay ratios have lower width to depth ratios (Schumm, 2003, p. 109), lower slopes (Schumm, 2003, p. 112) and are more likely to have a meandering rather than braided channel pattern (Ferguson, 1987). These morphological differences are believed to occur because of an increased resistance to erosion by turbulent flow and an increased mechanical strength against bank collapse. In contrast to estuarine and shallow-marine studies, and despite the importance of cohesive-sediment erosion and deposition to river morphology, relatively little work has been published on cohesive sediment transport in rivers.

Flood deposits in lateral separation eddies in the Colorado River in Marble and Grand Canyons emplaced prior to closure of Glen Canyon Dam in 1963 (Figure 1) often have a high percentage of silt and clay at their base and coarsen upwards (Topping *et al*., 2000). After closure of Glen Canyon Dam, all sediments supplied to the Colorado River in Marble and Grand Canyons come from tributaries downstream from the dam. Because closure of the dam cuts off the upstream supply of silt and clay, the Paria River is now the principal source of silt and clay to the Colorado River in Marble Canyon and the Paria and Little Colorado Rivers together are the principal sources of silt and clay to the Colorado River in Grand Canyon. The Paria River supplies only about 4% of the silt and clay that was supplied to the upstream end of Marble Canyon prior to closure of the dam, and the Paria River, Little Colorado River, and other small tributaries together only about 15–20% of the silt and clay that was supplied to the upstream end of Grand Canyon prior to closure of the dam (Topping *et al*., 2000; Webb *et al*., 2000). As a result of this large reduction in the amount of silt and clay supplied to the Colorado River in Marble and Grand Canyons, post-dam deposits in lateral separation eddies are typically much coarser than those formed prior to closure of the dam (Howard and Dolan, 1981; Topping *et al*., 2000).

*Correspondence to: Mark W. Schmeeckle, School of Geographical Sciences, Arizona State University, AZ, USA. E-mail: schmeeckle@asu.edu

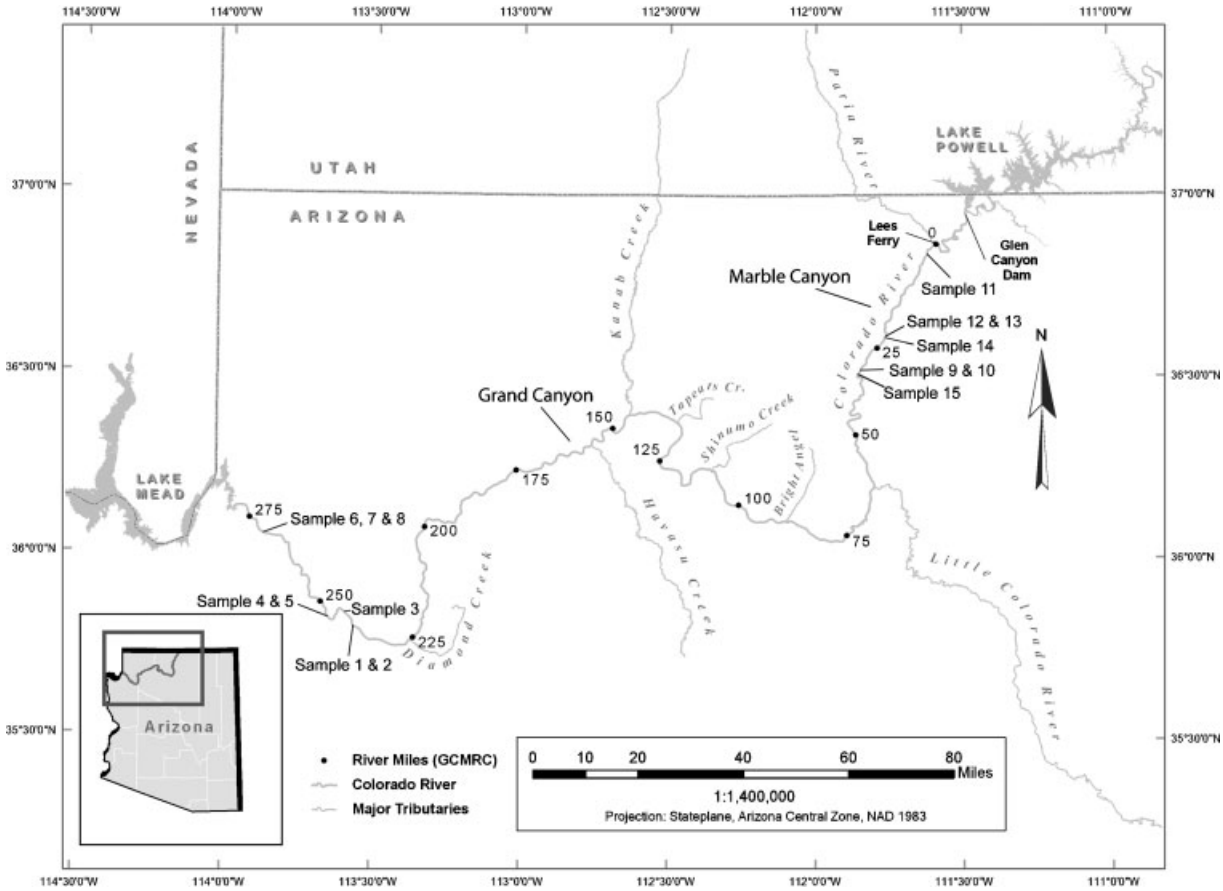

Figure 1. Location of sample collection sites along the Colorado River in the State of Arizona, USA. Marble Canyon is the portion of the Colorado River canyon between Glen Canyon Dam and the confluence of the Little Colorado River. Grand Canyon begins at the junction of the Little Colorado River and extends to the Grand Wash Cliffs at river mile 276. The maximum upstream extent of the Lake Mead backwater is at approximately river mile 235

Measurements of suspended sediment during the controlled-flood experiments of both 1996 and 2004 in Marble and Grand Canyons showed a sharp increase in silt and clay concentration during the rising limb of the flood hydrograph followed by a rapid decrease in concentration shortly after the hydrograph peak was reached (Topping *et al*., 2006). Because it did not follow a period of large tributary sediment inputs, the 1996 controlled-flood experiment occurred during a time when the Colorado River was relatively depleted with respect to sand, silt and clay. During the months leading up to the 2004 controlled-flood experiment, the Paria River and other tributaries supplied a large amount of sand, silt and clay. By the time of the 2004 controlled flood in late November, between 760 000 and 1 200 000 metric tons of sand and between 190 000 and 380 000 metric tons of silt and clay had accumulated below the Paria River in the first 47 km of the Colorado River in Marble Canyon. Because of the timing of the 2004 controlled-flood experiment during a period of relative sediment enrichment, suspended-silt and clay concentrations during the 2004 controlled flood were typically 2–3 times greater in Marble Canyon than they were during the 1996 controlled flood. Because of the greater amount of silt and clay in suspension in Marble Canyon, approximately three times the silt and clay was present in the 2004 deposits (16%) than in the 1996 deposits (∼5%). During both the 1996 and 2004 controlled floods, the amount of silt and clay in suspension decreased rapidly as the upstream supply became depleted. The relatively high concentration of silt and clay at the beginning of the flood peak led to the deposition of silt and clay at the base of the 2004 flood deposits. An example of the fine-grained layer at the base of the 2004 flood deposit at the 22 mile eddy is shown in Figure 2.

DOI: 10.1002/rra

Figure 2. Photograph of sediment deposited during the 2004 controlled-flood experiment in the reattachment bar at river mile 22. A scour chain can be seen below the base of the dark-coloured flood deposit. The dark coloured sediment is an indicator of a high percentage of silt and clay. The tape measure shown in the picture reads approximately 1.1 m at the top of the deposit. This figure is available in colour online at www.interscience.wiley.com/journal/rra

Although it was much greater than in the deposits formed during the 1996 controlled flood, the silt and clay content of the deposits formed during the 2004 controlled flood was much less than the content observed in the pre-dam deposits sampled by Topping *et al*. (2000). The one place in Grand Canyon where the silt and clay content of Colorado River deposits typically equals or exceeds the 40–70% level observed in the pre-dam deposits is the delta of the Colorado River in Lake Mead reservoir (Figure 1). The backwater profile of Lake Mead, which began filling in 1935 after construction of Hoover Dam, extends into the lower reach of Grand Canyon (Smith *et al*., 1960) and can reach as far as river mile 235. Low velocities in the backwater reaches between Separation Rapid and Lake Mead have led to deposition of a high percentage of silt and clay in bar and bank deposits. Thus, cohesive slab failure is common, and banks in this reach are steep. A predictive understanding of erosion of campsites and morphologic changes in the lower Grand Canyon will require a quantitative understanding of the sediment transport properties of Colorado River sediments with large percentages of silt and clay.

Cohesive sediment is not only important for the morphology of rivers, but also the riparian ecosystem. Erosion and transport of cohesive sediment increases the turbidity of the river water, which reduces the light available for autochthonous productivity (Thorp and Delong, 1994). Turbidity has in general been reduced leading to higher biomass production, particularly in the reach between Glen Canyon Dam and Lees Ferry (Angradi and Kubly, 1993). Fine-grained cohesive sediment also has a greater water holding capacity and increased nutrient concentrations relative to non-cohesive sediment, and the spatial distribution of marsh vegetation in Grand Canyon is related to the distribution of cohesive sediment (Stevens *et al*., 1995). Turbidity affects the assemblage composition and population of fish species in Grand Canyon directly through changes in predation (Marsh and Douglas, 1997), and indirectly by affecting the production and drift of the food base (Angradi, 1994; Shannon *et al*., 1996).

Unlike non-cohesive sediments, there are not any well-established relationships between flow and sediment entrainment and transport that do not require experimental calibration of the specific sediments of interest. Deposits containing a significant fraction of silt and clay are cohesive; electrochemical forces between grains must be broken

DOI: 10.1002/rra

in order to entrain the sediment into the overlying turbulent flow. Cohesion depends on the number of particle contacts per unit volume. Thus, smaller grain sizes have more particle contacts and higher cohesion than larger grain sizes. Mineralogical characteristics are important as well; the sheet silicate structure of clay minerals leads to particularly strong electrical interparticle bonds. As a deposit consolidates and increases in bulk density, the number of interparticle contacts per unit volume increases, which increases the cohesive strength of the deposit. The pH and ion content of the interstitial water affects the electro-chemical forces between grains and can, thus, be an important factor. Biological factors can be particularly important in reducing the erodibility of marine and estuarine muds. Of particular importance is the excretion of extracellular polymer substances (EPS) to form cohesive biofilms (Black *et al*., 2002). Due to the rapid deposition of sediments in the Colorado River, it is doubtful that there is sufficient time for the formation of these cohesive biofilms, and this study is based on the assumption that EPS and other biologic cohesive agents are relatively unimportant.

Unlike many marine and estuarine environments, any potentially cohesive sediment deposits along the Colorado River in Grand Canyon can be expected to contain a significant percentage of sand. Previous experiments have shown that the threshold boundary shear stress for erosion increases significantly when the silt and clay content is above about 30% (Panagiotopoulos *et al*., 1997). Van Ledden *et al*. (2004) argue that the transition between cohesive and non-cohesive sand/mud mixtures occurs at a clay content of between 5% and 10% and that silt content plays a minor role in determining cohesive behaviour. They argue that silt plus clay content is a useful predictor of cohesive behaviour only because most natural deposits exhibit a limited range of silt to clay ratios. Despite recent research on sand/mud mixtures (e.g. Barry *et al*., 2006), no reliable sediment erosion equations have been proposed that do not require experimental calibration of parameters.

The purpose of this study is to conduct controlled laboratory experiments on potentially cohesive sediments in the Colorado River in Grand Canyon to build an empirical erosion model. Such an erosion model could be used for the myriad of geomorphic and ecological issues in Grand Canyon restoration efforts (U.S. Department of the Interior, 1995; Gloss *et al*., 2005). The measurements and analysis also add to the relatively sparse information available on the erosion of cohesive sediment in rivers.

SAMPLE COLLECTION

Sediment samples were taken from the lower reach of Grand Canyon (within the delta of Lake Mead), from the surface of the 30-mile reattachment sandbar and from the base of the 2004 controlled-flood deposits (Figure 1). A number of samples tested in this study were collected in the lower Grand Canyon between Diamond Creek and Lake Mead (samples 1 through 8 in Table I). Bar and bank deposits in this reach are especially fine-grained because of reduction of flow velocity caused by the backwater profile of Lake Mead. When Lake Mead is nearly filled to capacity, the backwater curve extends as far upstream as river mile 236. Samples were collected between river mile 238 and 270 in February 2004. These samples were carefully cut from bar deposits, and then placed and sealed in rectangular $0.80 \times 0.40 \times 0.12\,\mathrm{m}^3$ plastic containers, so as not to disturb the structure of the cohesive sediments by breaking or mixing.

A second group of samples was collected in November 2004 from the surface of the 30-mile sandbar beach in Marble Canyon a day after emergence of the bar following the 2004 controlled-flood experiment. These samples were collected in 98 mm diameter by 77 mm, thin-walled (1 mm), stainless steel cylinders. The cylinders containing sediment samples were then placed in the laboratory flume for testing, thus avoiding further disturbance of the samples. Next to each flume sample, a smaller sample was taken for grain size analysis. Visual inspection of these samples from the surface of the bar at river mile 30 revealed that almost all of these samples contained little silt and clay. Thus only two of these samples were tested in the flume (samples 9 and 10 in Table I). Eddy bar deposits from the 2004 flood contained significant amounts of cohesive sediments only at the base of the flood deposit.

In the months following the 2004 controlled flood, a third group of samples was collected from the base of the 2004 flood deposits (samples 11 through 15 in Table I). Figure 2 shows the 2004 flood deposits at river mile 28. The dark colour at the base of the deposit is indicative of a high percentage of silt and clay. Samples were collected and sealed in plastic containers before being sent to the flume laboratory. These samples, as well as samples from the

DOI: 10.1002/rra

Table I. Grain size indices of Colorado River sediment samples

Sample no.	River mile	D_{50} (mm)	D_{84} (mm)	f_{clay}	f_{silt}	f_{mud}
1	238.6	0.08	0.15	0.08	0.37	0.45
2	238.6	0.04	0.15	0.10	0.47	0.57
3	241.5	0.04	0.14	0.13	0.45	0.58
4	246.2	0.04	0.12	0.13	0.54	0.67
5	246.2	0.04	0.12	0.13	0.50	0.63
6	270.6	0.08	0.19	0.19	0.24	0.43
7	270.6	0.13	0.21	0.08	0.17	0.25
8	270.6	0.06	0.17	0.22	0.28	0.50
9	30.8	0.22	0.38	0.00	0.02	0.02
10	30.8	0.18	0.25	0.02	0.02	0.04
11	2.6	0.16	0.22	0.04	0.08	0.11
12	22.0	0.05	0.14	0.07	0.47	0.53
13	22.0	0.16	0.28	0.04	0.20	0.24
14	22.3	0.07	0.17	0.07	0.40	0.47
15	31.7	0.05	0.13	0.05	0.54	0.59

River mile indicates the location at which the sample was collected (Fig. 1).

lower Grand Canyon, were not directly collected in the 98 mm diameter metal cylinders used in the laboratory flume, and, as such, were placed in the cylinders in the laboratory so as not to disturb the structure of the deposits.

Samples tested in the flume contained a broad range of percentages of silt and clay. Figure 3 shows the grain size distribution of the samples tested in the flume. The distribution of grain sizes larger than 0.075 mm was determined using dry sieve analysis. The distribution of grain sizes smaller than 0.075 mm was determined using hydrometer analysis following floc dispersion. Table I shows the median grain diameter, D50 and the grain diameter for which 84% of sediment in the sample is smaller than, D84. The fraction of clay, f_{clay}, the fraction of silt, f_{silt} and the fraction of mud, $f_{mud} \equiv f_{clay} + f_{silt}$, are also given in Table I. Even for sediments containing no organic material,

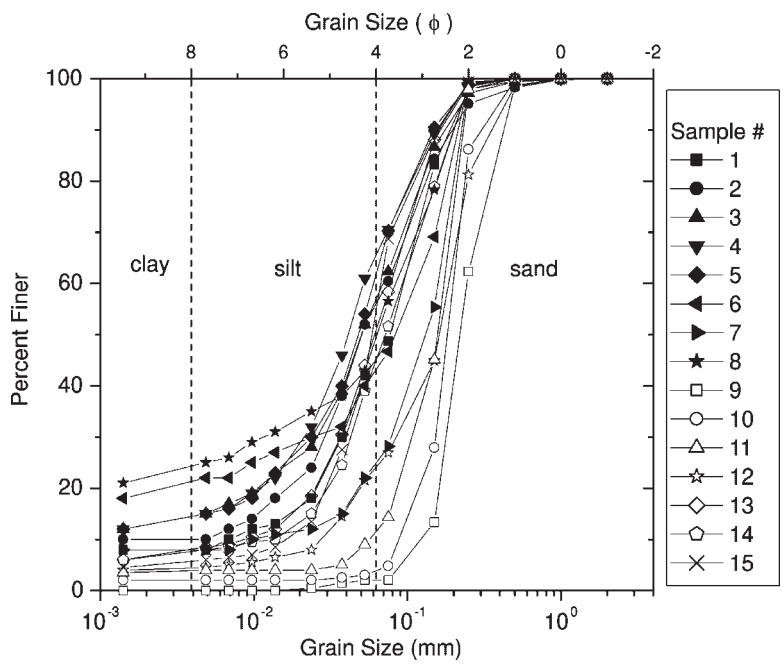

Figure 3. Grain size of Colorado River sediments tested in this study. Sample numbers correspond with those given in Table I

DOI: 10.1002/rra

there is no well-defined transition between cohesive and non-cohesive behaviour in terms of the concentration of clay and/or silt. According to Raudkivi (1998, p. 271), sediment becomes cohesive when the clay content exceeds about 10%. Given the broad range of factors such as clay mineralogy, water chemistry and depositional history, it is not surprising that there is no definitive method for dividing cohesive versus non-cohesive behaviour based upon the grain size distribution of a sample alone. Empirical testing of the erosion behaviour of representative samples from a given environment remains necessary.

Consolidation is known to reduce the erodibility of cohesive sediments. Bulk density provides a quantitative measure of consolidation, and previous laboratory experiments have shown that the bulk density of cohesive sediments from several rivers can be the most important factor in determining the amount of erosion at a given shear stress (Lick and McNeil, 2001). Consolidation of cohesive sediment under its own weight has been modelled by the Gibson consolidation equation (Gibson *et al*., 1967) which reduces to Terzaghi's consolidation equation (Terzaghi, 1943) during the final stages of dewatering when the strain rates become small (Winterwerp and van Kesteren, 2004). Consolidation ceases, in both the Gibson and Terzaghi consolidation equations, when the excess pore pressures become very small and the pore water pressures become hydrostatic. After the excess pore water pressures vanish, consolidation is largely the result of plastic deformation within the solid matrix. This secondary plastic deformation is generally very small except under very large overburden pressures. All samples collected in this study were only partially saturated, and thus finished with the primary stage of consolidation, and because all samples were collected at a depth of less than 2 m, it is unlikely that the samples experienced much secondary consolidation.

The saturated bulk densities of some of the sediment samples were tested. Not all samples were tested because of insufficient extra material for the test procedure. In this procedure, samples were collected in the same thin-walled cylinders used in the flume, then left underwater until fully saturated and weighed. The bulk density was then found by dividing the saturated mass by the volume of the sample. Table II shows results of this test. The samples are in the range between 1800 and 2000 kg m^{-3}. Assuming that the mineral grains and water have a density of 2600 and 1000 kg m^{-3}, respectively, the porosity of the sediment is in the range between 0.38 and 0.50.

EXPERIMENTS

The straight flume experiments of this study are similar to that of several previous studies (McNeil *et al*., 1996; Lick and McNeil, 2001; Witt and Westrich, 2003). In those and the present study a core of sediment was inset into the bed of a straight flume, and as the sediment was eroded, the sediment core was extruded so that the sediment surface remained at about the same height as the surrounding flume bed. Figure 4 is a photograph of the experimental flume used in this study, and Figure 5 schematically illustrates the experimental setup. The flume channel is made of Plexiglas and is 8.5 m long and 0.31 m wide. Water is stored in a downstream reservoir and is circulated by one or two centrifugal pumps. The discharge of one of the pumps is varied by an inverter. The sediment core sits within the stagnant water that fills the 0.15 m gap between a false floor and the main floor of the flume. The sediment cores are

Table II. Saturated bulk density of sediment samples

Sample no.	Saturated bulk density (kg m^{-3})
1	1810
2	1840
3	1870
4	1900
5	1910
6	2020
7	2010
8	2000

DOI: 10.1002/rra

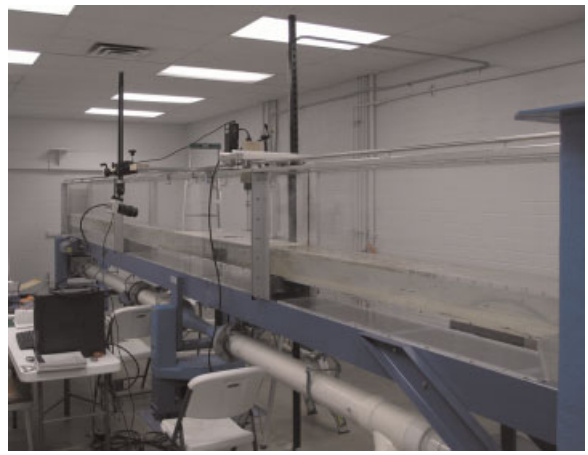

Figure 4. Photograph of the experimental setup. This figure is available in colour online at www.interscience.wiley.com/journal/rra

contained in a 77 mm long, thin-walled, stainless steel pipe section having an inner diameter of 98 mm. These cylinders are inset into a 100 mm hole bored in the false floor of the flume. Screws inset into the false bed of the flume are connected to a plate at the base of the core. Adjustment of these screws forces the sediment core to be extruded out of the false floor. Once a significant amount of sediment has been eroded, the flume discharge is stopped and the piston and sediment core are pushed upward, then the top part of the sample is cut to be flat and flush with the false floor. As a sample erodes, its surface moves below that of the false bed, which gradually decreases the rate of erosion. A number of initial tests were conducted to assure that sediment was extruded and levelled with the flume bed before a significant reduction in erosion rate occurred.

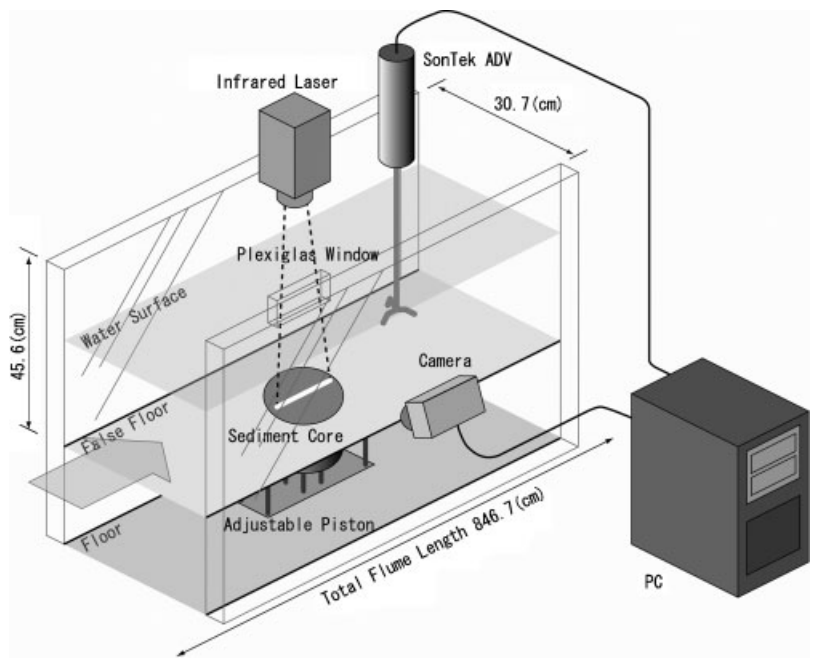

Figure 5. Illustrated diagram of the experimental setup

DOI: 10.1002/rra

Flow velocity approximately 1 cm above the bottom surface of the flume was measured by an Acoustic Doppler Velocimeter (Sontek Micro ADV), and boundary shear stress, τ_b, was calculated assuming the law of the wall over a hydraulically-smooth bed:

$$u = \frac{u_*}{k} \ln \frac{9u_* z}{\nu} \tag{1}$$

u is the time-averaged downstream velocity, u_* the friction velocity ($u_* \equiv \sqrt{\tau_b/\rho}$), k the von Karman's constant ($k = 0.41$), ν the kinematic viscosity and z is the height above the bed.

Erosion of the sediment surface was quantified using a simple digital photographic technique. A 1 mm thick near-infrared (810 nm) laser line was projected on the sediment surface from above the flume. The laser line was parallel with the long axis of the flume and ran through the centre of the core surface. The laser line was passed through a thin Plexiglas window at the water surface to avoid distortion by the moving water surface. A digital camera from the side of the flume having a slight angle relative to the bed surface imaged the laser line. Visible light was filtered by a near-infrared long pass filter on the camera lens, thus allowing for sharp delineation of the laser line at the sediment surface. A computer program was written to extract the lowest vertical pixel position of the laser line along the sample surface. This technique allowed detection of changes in bed elevation of less than 0.1 mm. The erosion velocity was calculated as the difference of this vertical position between images, averaged over the sample surface, and then divided by the time interval between successive images. It should be noted that in most studies of non-cohesive sediment transport in rivers, the erosion rate generally refers to the lowering of the sediment surface per unit time and has units LT^{-1} and will be called the erosion velocity in this study. In most cohesive sediment studies, the erosion rate refers to the rate of mass removed from a surface and has units $ML^{-2}T^{-1}$, and will be referred to as the mass erosion rate, E, in this study. The mass erosion rate can be found by multiplying the erosion velocity by the dry bulk density of the sediment.

Sample disturbance and water chemistry considerations

Mechanical disturbance of sediment deposits or change of the chemistry of the interstitial water is known to affect the erosion properties of cohesive sediments. Also the cohesive nature of some sediment is largely due to biological agents, and biofilms near the sediment surface can significantly increase the erosion threshold. These factors have led to the development of a number of instruments for erosion testing of cohesive sediments *in situ* (Amos *et al*., 1992; Maa *et al*., 1993; Black and Cramp, 1995; Widdows *et al*., 1998; Tolhurst *et al*., 1999; Aberle *et al*., 2003; Bale *et al*., 2006). These devices are placed directly on the cohesive sediment bed in the field, and as such, reduce the possibility of bed disturbance and alteration of chemical and biological conditions. Perhaps resulting from the difficulty in replicating the flow and turbulence in *in situ* devices, the correspondence of the critical shear stress for erosion among different types of *in situ* devices remains poor (Widdows *et al*., 2007). Furthermore, most *in situ* devices only measure the critical erosion threshold and cannot measure entrainment rates. Importantly, most of the sediments sampled in this study could not be studied *in situ* because they were at the base of flood deposits or on exposed bars. As well, samples taken from the base of flood deposits were deposited and buried in a matter of hours, which would presumably limit the possibility of biologically produced cohesive material. Finally, because the samples had already undergone the primary stage of consolidation, mechanical disturbance and further consolidation of the samples was minimal.

Cohesion of mineral grains occurs by electrochemical attraction between their surfaces. Clay minerals can form particularly strong electrical bonds because of their crystalline sheet structure. In very close proximity, the repulsive force between two likewise electrically charged surfaces can be overcome by attractive van der Waals forces. Ions in the water between two likewise charged surfaces reduce the electrical repulsive force and allow the surfaces to come into close enough proximity for van der Waals attractive forces to become dominant, and for clays to form strong edge-to-face electrical bonds. The ion content of water is particularly important in the flocculation and settling of cohesive sediments and is also important during erosion. The negative charge of a mineral surface attracts cations which reduce the negative electrical field with distance from the mineral surface. The effective distance of the electrical attraction between mineral grains is the thickness, λ, of the diffuse double layer (see Mitchell (1976) for an excellent review of double layer theory and the electrochemical forces between mineral

DOI: 10.1002/rra

grains). This thickness decreases with increasing molar concentration, c, of cations, and cation valence, υ, in the double layer (specifically: $\lambda \propto \upsilon^{-1} c^{-1/2}$). When cation concentration and valence are high, the double layer thickness is low and cohesion is high. Two-valence cations (primarily Ca and Mg) reduce the width of the diffusive double layer between grains more than single valence cations (primarily Na). Higher valence cations are more readily adsorbed in the double layer, and therefore, the ratio of single to double valence cations in the double layer is much lower than the ratio in the interstitial fluid and is proportional to the Sodium Adsorption Ratio (SAR):

$$\frac{[\mathrm{Na}^+]_a}{[\mathrm{Ca}^{2+}]_a + [\mathrm{Mg}^{2+}]_a} = k_1 \frac{[\mathrm{Na}^+]_i}{\sqrt{0.5([\mathrm{Ca}^{2+}]_i + [\mathrm{Mg}^{2+}]_i)}} = k_1(\mathrm{SAR}) \tag{2}$$

where ion concentrations are in milliequivalents per litre, and k_1 is a constant equal to approximately $0.017\,\mathrm{meq\,l^{-1}}$ for a broad range of minerals (Mitchell, 1976, p. 133). The subscripts i and a refer to concentrations in the interstitial fluid and the adsorbed double layer, respectively. The average concentration of Na, Ca and Mg in the laboratory water was 150, 53 and $22\,\mathrm{mg\,l^{-1}}$ (City of Tempe, 2007), and for the Colorado River at the USGS NASQAN site above Diamond Creek in water years from 1996 to 2005 the median concentration of Na, Ca and Mg was 73, 65 and $23\,\mathrm{mg\,l^{-1}}$ (United States Geological Survey, 2006). After some calculation using these values, the effective valence, υ, of the laboratory and Colorado River water is 1.85 and 1.93, respectively. The molar concentration of cations in laboratory and Colorado River water is 8.75 and $5.75\,\mathrm{mmol\,l^{-1}}$, respectively. Thus, the product, $\upsilon^{-1} c^{-1/2}$, is 0.18 and 0.22 for laboratory and Colorado River water. This means that the double layer thickness of the laboratory water may be slightly (about 20%) smaller and the cohesion slightly greater than the Colorado River water.

The pH of interstitial water is also known to affect the cohesion of clay particles. Conveniently, the pH of Colorado River water and the City of Tempe, Arizona tap water available in the flume laboratory are roughly equivalent. The median pH at the Diamond Creek NASQAN site on the Colorado River in the water years from 1996 to 2005 was 8.2 (United States Geological Survey, 2006), and the average pH in Tempe tap water in 2005 was 7.8 (City of Tempe, 2007). The erosion threshold results of Kandiah (1974) as redrawn in Winterwerp and van Kesteren (2004) under varying water salinities, SAR and pH conditions show that differences in the chemistry of the laboratory and Colorado River water should result in negligible differences in the erosion behaviour of the sediment samples.

RESULTS AND ANALYSIS

The basic results of erosion velocity versus boundary shear stress for all samples are shown in Figure 6. Contrary to what might be expected, it is apparent in Figure 6 that not all erosion rates were positive. This occurred as a minor amount of sediment was recirculated in the flume and could collect in small pits in the sample surface. Efforts to completely eliminate all recirculating sediments were unsuccessful. However, it is doubtful that the results were seriously compromised, as this minor sediment accumulation was far less than erosion velocities above the critical threshold.

Critical erosion threshold

Although there was a broad range of percentages of mud in the samples in Figure 6, all samples have only positive, and mostly sharply increasing erosion rates at boundary shear stresses above between 0.2 and 0.4 Pa. Apparently, there is a boundary shear stress erosion threshold, τ_e, in this range for all tested samples. A critical erosion boundary shear stress, τ_e, was found for each sample by averaging the boundary shear stress before and after the erosion rate became positive and remained positive for successively higher stresses.

It is instructive to compare the measured non-dimensional erosion threshold boundary shear stress, τ_{*e}, with the non-dimensional critical boundary shear stress for non-cohesive sediment, τ_{*c}. For this purpose, the Shields curve

DOI: 10.1002/rra

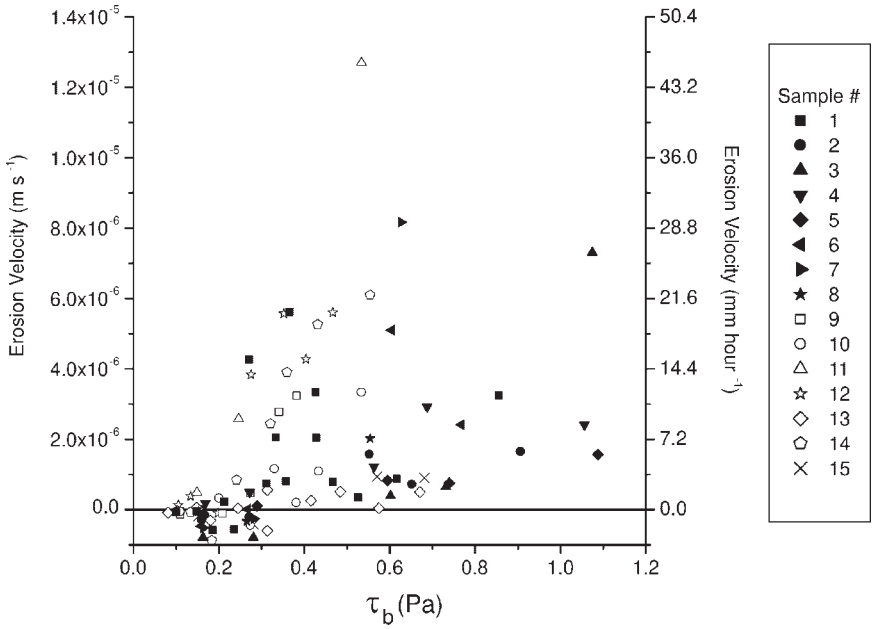

Figure 6. Erosion velocity versus boundary shear stress for all Colorado River samples. Sample numbers correspond with those given in Table I with sample collection locations shown in Figure 1

which gives, τ_{*c}, as a function of Reynolds roughness number, $\mathrm{Re} = u_* D/\nu$, is generally used. Equivalently, the Shields curve can be plotted explicitly with τ_{*c} as a function non-dimensional grain size, D_*, where

$$D_* \equiv \frac{\sqrt{\left(\frac{\rho_s}{\rho} - 1\right) g D^3}}{\nu} \tag{3}$$

Often the empirical function of Brownlie (1981) is used to model the original Shields diagram. However, for the purposes here, it is important that the smaller grain sizes of the Shields curve are adequately fit by the model function. Cao *et al*. (2006) point out that the original Shields diagram and Brownlie's function poorly fit the available data of the critical boundary shear stress for sizes smaller than fine sand, and they have proposed the following empirical function:

$$\begin{aligned} \tau_{*c} &= 0.1414 D_*^{-0.2306} && \text{when} \quad D_* \le 6.61 \\ \tau_{*c} &= \frac{\left[1 + (0.0223 D_*)^{2.8358}\right]^{0.3542}}{3.0946 D_*^{0.6769}} && \text{when} \quad 6.61 < D_* < 282.84 \\ \tau_{*c} &= 0.045 && \text{when} \quad D_* \ge 282.84 \end{aligned} \tag{4}$$

This function is plotted in Figure 7. The experimentally measured values of τ_*e are plotted on Figure 7 as well using the median grain size, D_{50}, of the sample in Equation 4. There is a clear deviation of τ_{*e} from the modelled Shields curve for samples with smaller grain sizes, whereas the four samples with the largest D_* are very close to the modelled Shields curve. It should be noted that Figure 7 is a log–log plot, and, thus τ_{*e} is often more than several times larger than τ_{*c}. Presumably, the difference between τ_{*e} and τ_{*c} results from cohesion. Correlation coefficients between the difference τ_{*e}–τ_{*c} and f_{clay}, f_{silt} and f_{mud} were calculated as 0.51, 0.74 and 0.77, respectively. Apparently, the fraction of silt plus clay is somewhat more useful in predicting the cohesiveness of sediments in this study than either fraction alone. The difference, τ_{*e}–τ_{*c}, is plotted as a function of f_{mud} in Figure 8. These data

DOI: 10.1002/rra

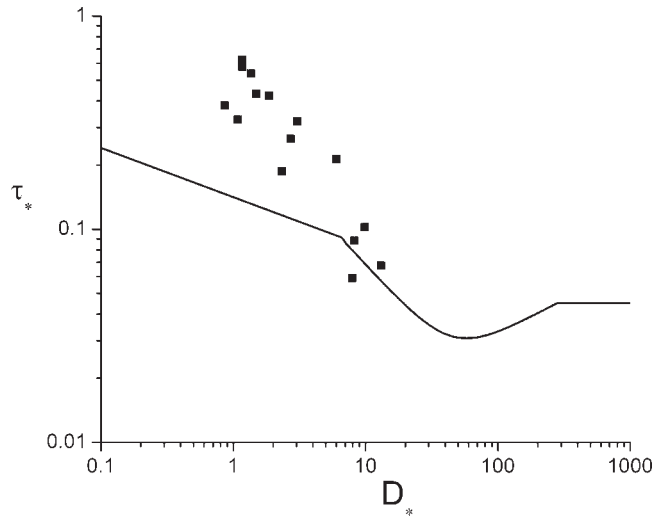

Figure 7. Non-dimensional critical erosion threshold, τ_*e, for all samples as a function of non-dimensional grain size, D_*. The equation of Cao *et al*. (2006) (Equation 4) for the non-dimensional critical shear stress for non-cohesive sediment is also plotted for comparison

suggest that cohesion becomes non-negligible when the amount of silt and clay is greater than about 20% ($f_{\mathrm{mud}} > 0.2$). A linear, least-squares fit of the data with $f_{\mathrm{mud}} > 0.2$ was performed ($R^2 = 0.42$, $p = 0.019$), and led to the following relationship, which is also plotted in Figure 8:

$$\begin{aligned} \tau_{*\mathrm{e}} &= \tau_{*\mathrm{c}} + 0.81(f_{\mathrm{mud}} - 0.2) \quad \text{when} \quad f_{\mathrm{mud}} > 0.2 \\ \tau_{*\mathrm{e}} &= \tau_{*\mathrm{c}} \qquad\qquad\qquad\qquad\quad \text{when} \quad f_{\mathrm{mud}} \leq 0.2 \end{aligned} \tag{5}$$

Mass erosion rate

A number of mass erosion rate relations have been proposed for cohesive sediments. Perhaps the most often used is the Ariathurai–Partheniades equation (Partheniades, 1962; Ariathurai, 1974)

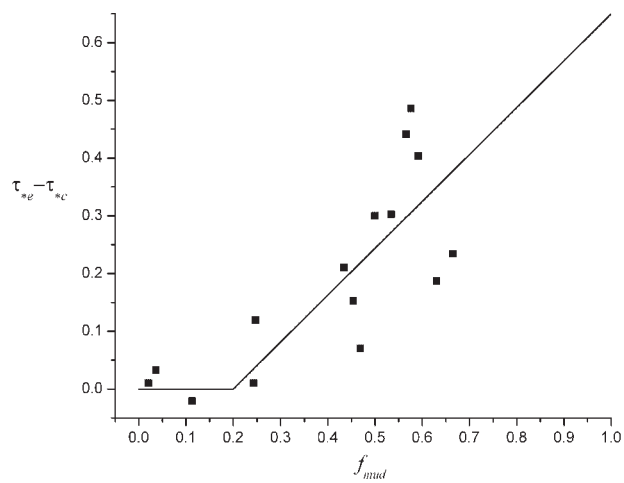

Figure 8. Difference between the non-dimensional critical erosion shear stress and the non-dimensional critical shear stress for non-cohesive sediment, $\tau_*e - \tau_*c$, as a function of mud fraction, f_{mud}. Equation 5 is also plotted

DOI: 10.1002/rra

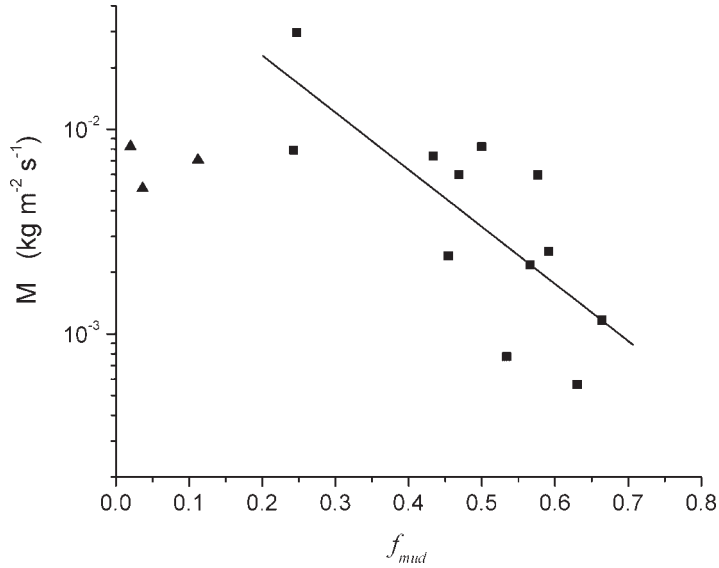

Figure 9. Erosion rate parameter, M, as a function of mud fraction, f_{mud}. Square symbols are used to plot samples which have mud fractions greater than 0.2, and triangles are used for samples having mud fractions less than 0.2. Equation 7 is also plotted

$$\begin{aligned} E &= M\left(\frac{\tau_b - \tau_e}{\tau_e}\right) \quad \text{when} \quad \tau_b > \tau_e \\ E &= 0 \qquad\qquad\qquad\quad \text{when} \quad \tau_b \leq \tau_e \end{aligned} \tag{6}$$

where E is the mass erosion rate per unit area, and M is an erosion rate parameter having the same units as E. The mass erosion rate, E, was determined from the measured erosion velocity assuming a dry bulk density of $1430\,\text{kg m}^{-3}$. Using the erosion rate data greater than τ_e, a linear, least-squares method was used to determine M for each sample tested in the flume. M is plotted as a function of mud fraction, f_{mud}, in Figure 9. This plot shows that there is a rapid decrease in the erosion rate with increasing mud fraction above 0.2. The ''non-cohesive'' samples having $f_{\text{mud}} < 0.2$ are plotted as triangles in the graph. Winterwerp and van Kesteren (2004) report that typical values of M are between 1×10^{-5} and $5 \times 10^{-4}\,\text{kg m}^{-2}\,\text{s}^{-1}$, which is lower than all but two of the most cohesive values found here, but Ariathurai and Arulanandan (1978) report values of M between 0.5×10^{-3} and $5 \times 10^{-3}\,\text{kg m}^{-2}\,\text{s}^{-1}$, which is similar to the values found here. Interestingly, the highest value of the erosion rate parameter is obtained by a sample with a mud fraction of 0.25, which is in the cohesive range. Apparently, the sediment cohesion at this mud fraction is not strong enough to offset the fact that the median grain size is much smaller than the non-cohesive samples. A log-linear equation ($R^2 = 0.58$, $p = 0.0042$) shown in Figure 9 was used to fit the cohesive samples, resulting in:

$$M = 0.083 \exp(-6.43 f_{\text{mud}}) \tag{7}$$

where M is given in units of $\text{kg m}^{-2}\,\text{s}^{-1}$.

As the bulk density of a deposit increases by consolidation, so should the critical erosion threshold, τ_e, and the erosion rate parameter, M. The correlation coefficients between bulk density (Table II) and τ_e and M are 0.34 and 0.61, respectively. Neither of these correlations are statistically significant at the 95% confidence level ($p = 0.41$ and 0.11, respectively). The reason for the lack of a significant correlation between bulk density and erosion parameters is perhaps because all of the collected samples had completed the primary stage of consolidation, as discussed earlier. This can be seen in the high and fairly limited range of bulk densities of the samples (Table II). Bulk density may be an important factor for newly deposited sediments in the Colorado River that continue to have excess pore water pressures, but the importance of bulk density cannot be investigated with samples collected in this study.

DOI: 10.1002/rra

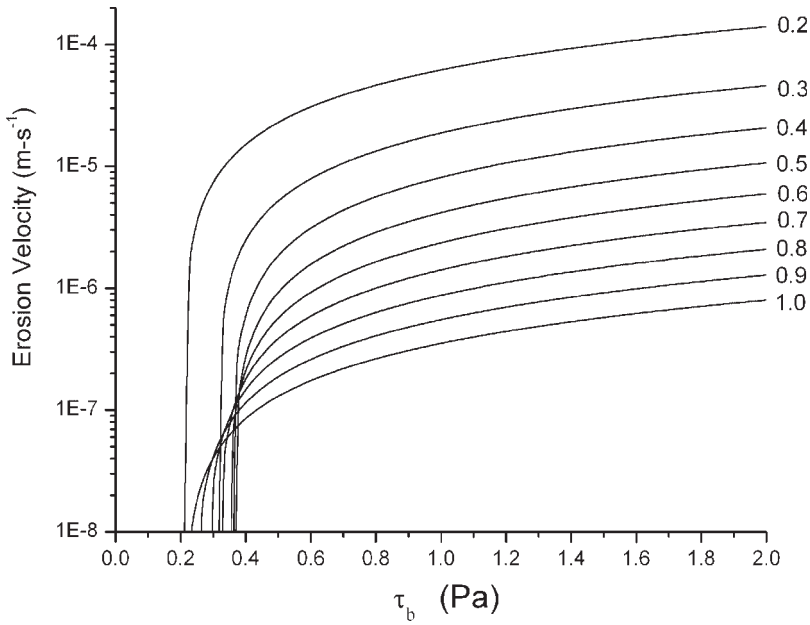

Figure 10. Erosion velocity is plotted as a function boundary shear stress for mud fractions between 0.2 and 1.0 using Equations 3 through 8

DISCUSSION AND CONCLUSIONS

Equations 3 through 7 can be used to model the erosion of consolidated cohesive sediments in the Colorado River in Grand Canyon. These equations require two grain size parameters, f_{mud} and D_{50}, which not surprisingly are highly negatively correlated ($r = -0.98$). The log-linear relation ($R^2 = 0.96$, $p < 0.0001$) with D_{50} in millimetres:

$$D_{50} = 0.24 \exp(-0.275 f_{\text{mud}}) \tag{8}$$

can be used to reduce the required number of input parameters.

Figure 10 is a plot erosion rate versus boundary shear stress using Equations 3 through 8 for various mud fractions. The erosion rate of sediment containing significant amounts of silt and clay is as much as two orders of magnitude lower than non-cohesive sediment, even at boundary shear stresses well above the erosion threshold. Thus cohesive deposits may erode at critical shear stresses roughly equivalent to the initiation of motion of non-cohesive fine or very fine sand deposits, but, in situations where the sediment transport rate is less than the transport capacity, cohesive deposits will erode much less rapidly. The less-rapid erosion of cohesive sediment deposits would lead to a sustained period of increased turbidity.

These factors are relevant when considering the erosion of pre-dam versus post-dam deposits and may be useful for future dam operations. Colorado River Grand Canyon flood deposits in lateral separation eddies prior to construction of Glen Canyon Dam often had mud fractions in the range between 0.4 and 0.7 (Topping *et al.*, 2000), whereas post-dam deposits have mud fractions that are typically less than 0.2. Under similar stage and upstream sediment supply conditions, pre-dam cohesive sediments would erode much less rapidly than post-dam deposits. Promotion of deposition of higher mud fractions during controlled floods may lead to a somewhat greater degree of bar stability and an increased period of higher turbidity.

ACKNOWLEDGEMENTS

This work was funded in part by the National Science Foundation under award number EAR-0352079, and by cooperative agreement number 05WRAG0047 between the U.S. Geological Survey, Southwest Biological Science

DOI: 10.1002/rra

Center, Grand Canyon Monitoring and Research Center and Arizona State University. We wish to thank Noah Snyder, Neil Ganju and one anonymous reviewer for helping us improve this manuscript.

REFERENCES

Aberle J, Nikora V, Mclean S, Doscher C, McEwan I, Green M, Goring D, Wash J. 2003. Straight benthic flow-through flume for in situ measurement of cohesive sediment dynamics. *Journal of Hydraulic Engineering-Asce* **129**: 63–67.

Amos CL, Daborn GR, Christian HA, Atkinson A, Robertson A. 1992. In situ erosion measurements on fine-grained sediments from the Bay of Fundy. *Marine Geology* **108**: 175–196.

Angradi TR. 1994. Trophic linkages in the lower Colorado River - multiple stable-isotope evidence. *Journal of the North American Benthological Society* **13**: 479–495.

Angradi TR, Kubly DM. 1993. Effects of atmospheric exposure on chlorophyll-a, biomass and productivity of the Epilithon of a Tailwater River. *Regulated Rivers-Research & Management* **8**: 345–358.

Ariathurai R. 1974. A finite element model for sediment transport in estuaries. Ph.D. Dissertation. University of California, Davis.

Ariathurai R, Arulanandan K. 1978. Erosion rates of cohesive soils. *Journal of the Hydraulics Division-Asce* **104**: 279–283.

Bale AJ, Widdows J, Harris CB, Stephens JA. 2006. Measurements of the critical erosion threshold of surface sediments along the Tamar Estuary using a mini-annular flume. *Continental Shelf Research* **26**: 1206–1216.

Barry KM, Thieke RJ, Mehta AJ. 2006. Quasi-hydrodynamic lubrication effect of clay particles on and grain erosion. *Estuarine Coastal and Shelf Science* **67**: 161–169.

Black K, Cramp A. 1995. A device to examine the in situ response of intertidal cohesive sediment deposits to fluid shear. *Continental Shelf Research* **15**: 1945–1954.

Black KS, Tolhurst TJ, Paterson DM, Hagerthey SE. 2002. Working with natural cohesive sediments. *Journal of Hydraulic Engineering-ASCE* **128**: 2–8.

Brownlie WR. 1981. Prediction of flow depth and sediment discharge in open-channels. W. M. Kech Lab. Hydraulics and Water Resources, California Institute of Technology, Pasadena, California.

Cao ZX, Pender G, Meng J. 2006. Explicit formulation of the Shields Diagram for incipient motion of sediment. *Journal of Hydraulic Engineering-Asce* **132**: 1097–1099.

City of Tempe. 2007. 2005 Water-Quality Report: URL http://www.tempe.gov/waterquality/ccr/CCR2005.pdf [Accessed 18 June 2007].

Ferguson RI. 1987. Hydraulic and sedimentary controls of channel pattern. In *River Channels: Environment and Process*. KS Richards (ed). Blackwell: Oxford 125–158.

Gibson RE, England GL, Hussey MJL. 1967. The theory of one dimensional consolidation of saturated clays, I. Finite non-linear consolidation of thin homogeneous layer. *Geotechnique* **17**: 261–273.

Gloss SP, Lovich JE, Melis TS. 2005. The state of the Colorado River ecosystem in Grand Canyon. *US Geological Survey Circular* **1282**: 1–220.

Howard A, Dolan R. 1981. Geomorphology of the Colorado River in the Grand-Canyon. *Journal of Geology* **89**: 269–2298.

Kandiah A. 1974. Fundamental aspects of surface erosion of cohesive soils. Ph.D. Dissertation. University of California, Davis.

Lick W, McNeil J. 2001. Effects of sediment bulk properties on erosion rates. *Science of the Total Environment* **266**: 41–48.

Maa JPY, Wright LD, Lee CH, Shannon TW. 1993. Vims sea carousel—a field instrument for studying sediment transport. *Marine Geology* **115**: 271–287.

Marsh PC, Douglas ME. 1997. Predation by introduced fishes on endangered humpback chub and other native species in the Little Colorado River, Arizona. *Transactions of the American Fisheries Society* **126**: 343–346.

McNeil J, Taylor C, Lick W. 1996. Measurements of erosion of undisturbed bottom sediments with depth. *Journal of Hydraulic Engineering-ASCE* **122**: 316–324.

Mitchell JK. 1976. *Fundamentals of Soil Behavior.* John Wiley & Sons: New York.

Panagiotopoulos I, Voulgaris G, Collins MB. 1997. The influence of clay on the threshold of movement of fine sandy beds. *Coastal Engineering* **32**: 19–43.

Partheniades E. 1962. A study of erosion and deposition of cohesive soils in salt water. Ph.D. Dissertation. University of California, Berkeley.

Raudkivi AJ. 1998. *Loose Boundary Hydraulics*. Balkema: Rotterdam, Netherlands.

Schumm SA. 2003. *The Fluvial System*. The Blackburn Press Caldwell, New Jersey, USA.

Shannon JP, Blinn DW, Benenati PL, Wilson KP. 1996. Organic drift in a regulated desert river. *Canadian Journal of Fisheries and Aquatic Sciences* **53**: 1360–1369.

Smith WO, Vetter CP, Cummings GB. 1960. Comprehensive survey of sedimentation in Lake Mead, 1948–1949, US Geological Survey Professional Paper 295.

Stevens LE, Schmidt JC, Ayers TJ, Brown BT. 1995. Flow regulation, geomorphology, and Colorado-River marsh development in the Grand-Canyon, Arizona. *Ecological Applications* **5**: 1025–1039.

Terzaghi K. 1943. *Theoretical Soil Mechanics*. John Wiley and Sons: New York.

Thorp JH, Delong MD. 1994. The riverine productivity model—an heuristic view of carbon-sources and organic-processing in large river ecosystems. *Oikos* **70**: 305–308.

Tolhurst TJ, Black KS, Shayler SA, Mather S, Black I, Baker K, Paterson DM. 1999. Measuring the in situ erosion shear stress of intertidal sediments with the cohesive strength meter (Csm). *Estuarine Coastal and Shelf Science* **49**: 281–294.

DOI: 10.1002/rra

Topping DJ, Rubin DM, Vierra LE. 2000. Colorado River sediment transport—1. Natural sediment supply limitation and the influence of Glen Canyon Dam. *Water Resources Research* **36**: 515–542.

Topping DJ, Rubin DM, Schmidt JC, Hazel JE, Melis TS, Wright SA, Kaplinski M, Draut AE, Breedlove MJ. 2006. Comparison of Sediment-Transport and Bar-Response Results from the 1996 and 2004 Controlled-Flood Experiments on the Colorado River in Grand Canyon. *Proceedings of the Eighth Federal Interagency Sedimentation Conference*.

U.S. Department of the Interior. 1995. Operation of Glen Canyon Dam Final Environmental Impact Statement: Salt Lake City, Utah, Bureau of Reclamation, Upper Colorado Region. 337.

United States Geological Survey. 2006. National Stream Water Quality Network (NASQAN), Summary Statistics for NASQAN Data–Colorado Basin 1997–2005, Colorado River at Diamond Creek, Arizona (09404200): URL http://water.usgs.gov/nasqan/data/statsum/diamond.html [Accessed 25 July 2007].

Van Ledden M, Van Kesteren WGM, Winterwerp JC. 2004. A conceptual framework for the erosion behaviour of sand-mud mixtures. *Continental Shelf Research* **24**: 1–111.

Webb RH, Griffiths PG, Melis TS, Hartley DR. 2000. Sediment delivery by ungaged tributaries of the Colorado River in Grand Canyon, Arizona. *U.S. Geological Survey Water-Resources Investigations Report*: 004055.

Widdows J, Brinsley MD, Bowley N, Barrett C. 1998. A benthic annular flume for in situ measurement of suspension feeding/biodeposition rates and erosion potential of intertidal cohesive sediments. *Estuarine Coastal and Shelf Science* **46**: 27–38.

Widdows J, Friend PL, Bale AJ, Brinsley MD, Pope ND, Thompson CEL. 2007. Inter-comparison between five devices for determining erodability of intertidal sediments. *Continental Shelf Research* **27**: 1174–1189.

Winterwerp JC, van Kesteren WGM. 2004. *Introduction to the Physics of Cohesive Sediment Dynamics in the Marine Environment*. Elsevier: Amsterdam; 466.

Witt O, Westrich B. 2003. Quantification of erosion rates for undisturbed contaminated cohesive sediment cores by image analysis. *Hydrobiologia* **494**: 271–276.

DOI: 10.1002/rra